Metabolic signature of ethanol-induced hepatotoxicity in HepaRG cells by LC-MS-based untargeted metabolomics

Elias Iturrospe [1,2,*], Katyeny Manuela da Silva [1], Rani Robeyns [1], Maria van de Lavoir [1], Joost Boeckmans [2], Tamara Vanhaecke [2], Alexander L.N. van Nuijs [1], Adrian Covaci [1,*]

[1] University of Antwerp, Toxicological Centre, Universiteitsplein 1, 2610 Antwerp, Belgium

[2] Vrije Universiteit Brussel, Department of *In Vitro* Toxicology and Dermato-cosmetology, Laarbeeklaan 103, 1090 Jette, Belgium

Corresponding Authors

* E-mail: adrian.covaci@uantwerpen.be, elias.iturrospe@uantwerpen.be

ABSTRACT

Alcoholic liver disease is highly prevalent but poorly identified and characterized, leading to knowledge gaps impairing early diagnosis. Excessive alcohol consumption is known to alter lipid metabolism, followed by progressive intracellular lipid accumulation, resulting in alcoholic fatty liver disease. In this study, HepaRG cells were exposed to ethanol at IC_{10} and 1/10 IC_{10} for 24 h and 48 h. Metabolic alterations were investigated intra- and extracellularly with liquid chromatography – high-resolution mass spectrometry. Ion mobility was added as an extra separation dimension for untargeted lipidomics to improve annotation confidence. Distinctive patterns between exposed and control cells were consistently observed, with intracellular upregulation of di- and triglycerides, downregulation of phosphatidylcholines and -ethanolamines, sphingomyelins and S-adenosylmethionine amongst others. Several intracellular metabolic patterns could be related to changes in the extracellular environment, such as increased intracellular hydrolysis of sphingomyelins leading to increased phosphorylcholine secretion. Carnitines showed alterations depending on the size of their carbon chain which highlights the interplay between β-oxidation in mitochondria and peroxisomes. Potential new biomarkers of ethanol-induced hepatotoxicity have been observed, such as ceramides with a sphingadienine-backbone, octanoylcarnitine, creatine, acetylcholine and ethoxylated phosphorylcholine. The combination of the metabolic fingerprint and footprint enabled a comprehensive investigation of the pathophysiology behind ethanol-induced hepatotoxicity.

KEYWORDS: High-resolution mass spectrometry; Liquid chromatography; Drift tube ion mobility; Metabolomics; Lipidomics; Alcoholic liver disease; Hepatocytes; HepaRG; Steatosis; Alcohol

1. INTRODUCTION

Excessive alcohol use is a major causality of liver disease worldwide and the most common cause of acute-on-chronic liver failure.[1] About 2 billion people consume alcohol, and more than 75 million are diagnosed with alcohol-use disorders and are at risk of developing alcoholic liver disease (ALD).[1] Alcohol is known to alter fat metabolism processes, followed by progressive intracellular lipid accumulation, resulting in alcoholic fatty liver disease (AFLD).[2,3] AFLD can progress to alcoholic steatohepatitis (ASH), which is characterized by hepatic inflammation and hepatocellular ballooning. Chronic ASH can eventually lead to fibrosis and cirrhosis and, in some cases, to hepatocellular cancer.[2–6] Besides the slow progression of ASH to fibrosis and cirrhosis, a rapid progression to alcoholic hepatitis associated with a poor prognosis can occur.[3] A major challenge exists in the clinical diagnosis of ALD.[3,7] Alcohol-related disorders, which put individuals at high risk of developing ALD, are highly prevalent but poorly identified and characterized.[3] Symptoms tend to develop late in the course of disease progression and may only be apparent at the stage of irreversible cirrhosis.[3,7] There are no early and specific biomarkers for the diagnosis of ALD, and currently, no single marker or combination of markers can be used to differentiate between different causes and stages of liver disease.[8,9]

Because changes in the metabolome often are reflected in changes in the phenotype and vice-versa, metabolomics and its subdiscipline lipidomics offer the opportunity to identify diagnostic biomarkers, showcase potential pharmacotherapeutic targets and clarify the mechanism of action of ethanol-induced hepatotoxicity, with the overall objective to facilitate intervention in early stages of ALD. Untargeted metabolomics and lipidomics encompass the holistic investigation of low molecular weight (< 1500 Da) endogenous metabolites and provide information on the biochemical status of a biological system. While lipidomics is used to study lipids, metabolomic research typically involves more polar metabolites.[10] Based on relative differences in signal abundance between biological control samples and biological samples exposed to ethanol, the metabolic signature of ethanol exposure can be elucidated. Although animal models to study ethanol-induced hepatotoxicity are useful, they suffer from several drawbacks such as lower susceptibility of rodents to develop ALD and differences in the pathophysiological stages of ALD development compared to humans.[11,12]

In vitro hepatic metabolic research on the other hand enables mechanistic elucidation at the cellular level and circumvents the difficult accessibility of the liver through biopsies. Despite the consideration of primary hepatocytes to be the golden standard for *in vitro* applications, they suffer from limitations such as high inter-donor metabolic variability and limited *in vitro* stability.[13] The hepatic HepaRG cell line is a promising alternative due to low variability and long-term stability while maintaining expression of most liver-specific functions, such as cytochrome P450 (CYP) activity and bile acid synthesis. In addition, HepaRG cells are capable to differentiate towards hepatocyte-like cells and biliary-like cells, mimicking the *in vivo*

situation.[13,14] In this study, HepaRG cells, derived from a human hepatocellular carcinoma, were used to investigate the effects of ethanol exposure on cell metabolism using liquid chromatrography (LC)-MS-based untargeted metabolomics platforms. Extraction and analysis of intracellular metabolites were able to provide a metabolic fingerprint for ethanol-induced hepatotoxicity in HepaRG cells. In addition, conditioned cell media were analysed to yield the metabolic footprint (i.e., provide information on metabolic secretion and consumption).[15] Dynamic changes of metabolites were elucidated in order to get a better understanding of early-stage indicators of AFLD. Due to the high diversity of lipid isomeric structures, these latter were further investigated using ion mobility spectrometry (IMS) to improve the level of confidence in annotation at species-level.

2. EXPERIMENTAL SECTION

2.1. Materials and chemicals

Internal standards hippuric acid-(phenyl-$^{13}C_6$), L-lysine-$^{13}C_6$-$^{15}N_2$, Leucine-5,5,5-D_3, glucose-$^{13}C_6$, glyceryl tri(palmitate-1-^{13}C) and cholic acid-2,2,4,4-D_4 were purchased from Sigma Aldrich (St. Louis, Missouri, USA). Lauric acid-12,12,12-D_3 was bought from CDN Isotopes (Pointe-Claire, Quebec, Canada), caffeine-$^{13}C_3$ from Cerilliant Corporation (Texas, USA), 18:1-D_7 lyso PE from Avanti Polar Lipids and octanoyl-L-carnitine-(N-methyl-D_3), ceramide (d18:1/18:1(9Z)-$^{13}C_{18}$) and L-phenylalanine-$^{13}C_9$-^{15}N from Cambridge Isotope Laboratories (Massachusetts, USA). Methanol (MeOH), acetonitrile (ACN) and formic acid (99%, HCOOH), all ULC/MS-CC/CSF grade, were purchased from Biosolve (Valkenswaard, The Netherlands). Ammonium formate (≥ 99%, NH_4COOH) LC-MS grade, ammonium carbonate HPLC grade ($(NH_4)_2CO_3$) and ammonium acetate LC-MS grade (NH_4COOCH_3) were obtained from Sigma Aldrich. Acetic acid (100%, $HCOOCH_3$) and ammonia solution (25%, $NH_3(aq)$), both LC-MS grade, isopropanol for analysis (ACS reagent) (IPA) and chloroform (analytical grade) ($CHCl_3$), were purchased from Merck (Darmstadt, Germany). Ultrapure water (H_2O) used throughout the experiments was obtained from an Elga Pure Lab apparatus (Tienen, Belgium). L-ascorbic acid (≥ 99%), butylated hydroxytoluene (≥ 99%, BHT), EDTA (99.995%) and neutral red (BioReagent) were purchased from Sigma Aldrich.

Differentiated HepaRG cells, Basal Hepatic Medium, HepaRG Thaw, Seed and General-Purpose Supplement and HepaRG Maintenance and Metabolism Supplement were acquired from Biopredic International (Rennes, France). HepaRG cells were seeded in Permanox 2-well Lab-Tek chamber slides from Nunc, Thermo Scientific (Rochester NY, USA) and incubated using a Galaxy 170 S incubator acquired from Eppendorf (Hamburg, Germany). Rat tail collagen type I for coating was provided by Corning (New York, USA). 96-well plates from Falcon (Corning, New York, USA) were used for inhibitory concentration 10 (IC_{10}) determinations. Ethanol for cell exposure (≥ 99.8%, molecular biology, EtOH) was purchased from Sigma Aldrich. Eppendorf Safe-Lock tubes, Reacti-Vials and 0.2 µm nylon centrifugal

filters were acquired from Eppendorf, Thermo Scientific and VWR (Pennsylvania, USA), respectively. Pure, dry nitrogen (AZOTE N28, N_2) used for solvent evaporation was obtained from Air Liquide Belge (Liège, Belgium). 384-well plates (PS, small volume) were bought from Greiner Bio-One (Vilvoorde, Belgium).

2.2. Determination of the IC_{10} of ethanol

The IC_{10} of ethanol for HepaRG cells was determined for 24 h and 48 h of exposure via the neutral red uptake assay as described by Ates *et al.*[16] HepaRG cells were seeded in 96-well plates at a concentration of 94 x 10^3 cells per well. The cells were incubated for 7 days at 37 °C, 5% CO_2, and saturated humidity. On day 7, cells were divided into equal groups I and II, which were subject to 24 h and 48 h of ethanol exposure, respectively. Cells from groups I and II were exposed to eight different concentrations of ethanol (range 250-950 mM, increments of 100 mM) for 24 h. For cells of group II, ethanol-containing media were renewed after 24 h and exposure was continued for another 24 h. In addition, unexposed negative controls and blanks were obtained. After exposure, used media were replaced by neutral red-containing media (25 µg/mL) and incubation was continued for another 3 h. Media were washed away using phosphate-buffered saline (PBS, 37 °C), and a desorption solution was added to the cells (1% $HCOOCH_3$, 50% EtOH and 49% H_2O, v/v/v) after which they were shaken for 30 min at 80 rpm in a dark environment. After 5 min equilibration, absorption was measured at 540 ± 10 nm using a victor³ 1420 multilabel counter (Perkin Elmer, Massachusetts, USA). Experiments were conducted in triplicate. To avoid cross-contamination due to the volatile nature of EtOH, separate well plates were used for each concentration of EtOH and PBS containing the same EtOH concentration was used to fill surrounding wells. Absorbance was plotted against EtOH concentration, and the IC_{10} value was calculated using four-parameter logistics in Graphpad Prism (v. 9.0).

2.3. Sample collection and preparation

Ethical approval for the use of HepaRG cells was provided by the Medical Ethics Committee of the University Hospital Brussels (reference number 143201941214). HepaRG cells were seeded in collagen-coated Permanox 2-well Lab-Tek chamber slides at a concentration of 1 x 10^6 cells per well. The cells were incubated for 7 days at 37 °C, 5% CO_2, and saturated humidity. On day 7, cells were exposed to 368 mM of ethanol (i.e., IC_{10}, n = 6), 36.8 mM (i.e., 1/10 IC_{10}, n = 6) or no ethanol (i.e., negative control, n = 6) and cultivated for another 24 h. For the 48 h exposure group, cells were exposed to 284 mM of ethanol (i.e., IC_{10}, n = 6), 28.4 mM (i.e., 1/10 IC_{10}, n = 6) or no ethanol (i.e., negative control, n = 6) and cultivated for another 48 h with renewal of ethanol containing media after 24 h (Fig. 1). Negative control groups, sample groups exposed to the IC_{10} of ethanol and to 1/10 of the IC_{10} of ethanol will be further referred to as sample

groups C, H and L, respectively. In addition, two extraction blanks, not containing cells, were obtained for each exposure group using the same conditions. Due to the volatile nature of ethanol, concentration loss during cultivation was expected. More importantly, ethanol evaporation from cells exposed to a high concentration can cause cross-contamination of cells exposed to a low concentration or unexposed negative controls. Therefore, cells were cultivated in chamber slides within Petri dishes to minimize the risk of cross-contamination. Each chamber slide comprised two wells. Cells were exposed to ethanol-containing medium in one well, while PBS with the same ethanol concentration was added to the second well. In addition, the concentration of ethanol in the medium was determined before and after cultivation using headspace gas chromatography with flame ionization detection (HS-GC-FID). Extracts of HepaRG cells were prepared as previously described.[17,18] Briefly, cells were flash-frozen using liquid nitrogen and scraped from the carrier with a quenching solution of 80% MeOH and 20% 10 mM NH_4COOCH_3 (v/v) in H_2O at -80 °C. The same solution was used to quench the extracted incubation media. The quenching solution containing the scraped cells and the quenched media were recovered to perform liquid-liquid extraction (LLE) with a final solvent ratio of 3/2/2, MeOH/H_2O/$CHCl_3$ (v/v/v). A mixture of 12 internal standards was added (concentration after reconstitution 2 µg/mL). The upper and lower fractions were divided in two for the analysis in positive and negative electrospray ionization (ESI (+) and ESI (-), respectively. After drying under a N_2 stream at room temperature, extracts from the upper and lower fraction were reconstituted in ACN/H_2O (65/35, v/v) and IPA/MeOH (35/65, v/v) for metabolomics and lipidomics analysis, respectively. In addition, a separate quality control (QC) pooled sample was generated for each analytical platform, ionization mode, and exposure timepoint, by combining equal volumes of the samples, with the exception of extraction blanks. A detailed protocol of the sample collection and preparation can be found in SI-1. All exposure experiments were repeated to validate the experiment (Fig. 1), using a second batch of HepaRG cells (batch numbers were 116310 and 116308, respectively). Since cell samples (i.e., intracellular (IC) fraction) and conditioned media samples (i.e., extracellular (EC) fraction) were prepared separately, subsequent data acquisition and -analysis were used for metabolic fingerprinting and footprinting, respectively.

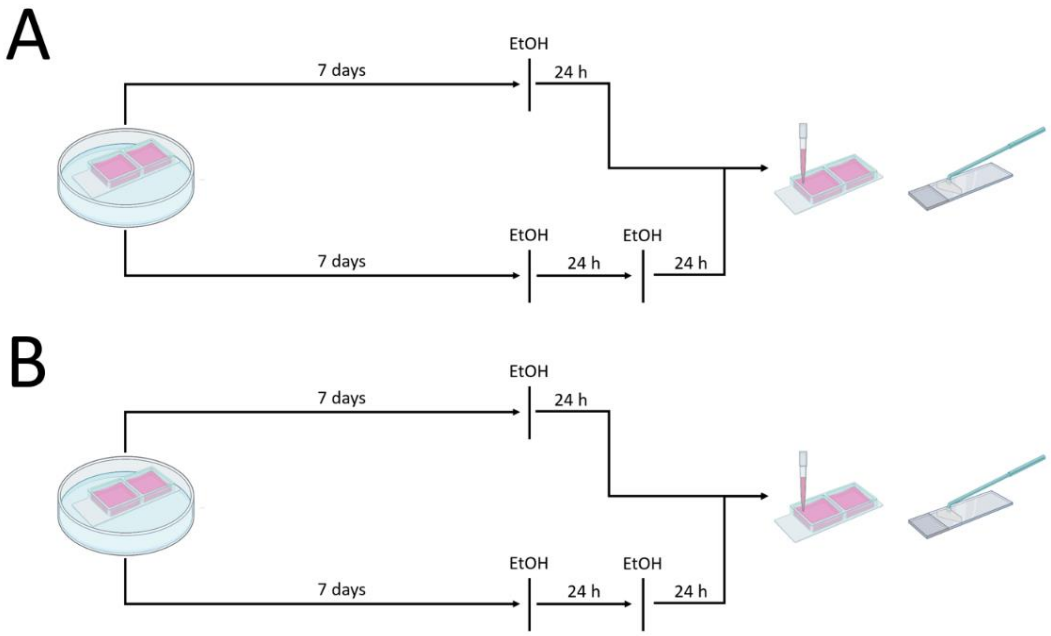

Fig. 1. Graphical representation of the exposure experiment (A) and the validation experiment (B). HepaRG cells were exposed to ethanol at the IC_{10} and 1/10 of the IC_{10} for 24 h and 48 h. The difference between (A) and (B) is the use of different batches of HepaRG cells.

2.4. HS-GC-FID data acquisition

To quantify ethanol in cell media, headspace analysis was performed on an Agilent 6890 gas chromatograph with an FID detector coupled to an Agilent 7697A headspace sampler (Agilent Technologies, Santa Clara, USA). An Agilent J&W DB-1 column (50 m x 0.32 mm x 1.2 µm) was used and the oven and detector temperatures were 175 and 250 °C, respectively. The validated method[19] used hydrogen as a carrier gas (67.8 mL/min total flow, 30:1 split ratio). The detector gas comprised of hydrogen (40 mL/min), air (300 mL/min) and nitrogen makeup (5 mL/min). Calibration was performed using six aqueous ethanol standards within a range of 0.05-5 g/L (ACQ Science GmbH, Rottenburg, Germany). For determination of the ethanol concentration in cultivated media, 400 µL of the medium was added to 1.5 mL H_2O and 100 µL ACN as internal standard (0.786 g/L). Samples with ethanol concentrations outside of the calibration range were diluted and re-analyzed. To ensure the analytical performance, ethanol QC solutions of 0.3 g/L and 4.0 g/L were analyzed before and after the run (ACQ Science GmbH).

2.5. LC-(DTIM)-HRMS data acquisition

Liquid chromatography (LC) – high-resolution mass spectrometry (HRMS) acquisition parameters used during metabolomics and lipidomics analyses and additional drift tube ion mobility (DTIM) parameters

used during lipidomics analyses were previously optimized by Iturrospe *et al.* and Da Silva *et al.*[17,18] Analytical measurements of the polar fraction of the samples were carried out on an Agilent 1290 Infinity UPLC system coupled to an Agilent 6530 quadrupole-time-of-flight (QToF) HRMS with Agilent Jet Stream Electrospray Ionization. In ESI (+), an iHILIC-Fusion column (100 x 2.1 mm, 1.8 µm, zwitterionic, charge modulated amide, silica-based, HILICON AB, Sweden) was used with 10 mM NH_4COOH and 0.1% (v/v) HCOOH in H_2O/MeOH (9/1, v/v) as mobile phase A (MPA) and ACN as mobile phase B (MPB). In ESI (-), an iHILIC-Fusion(P) column (100 x 2.1 mm, 5 µm, zwitterionic, charge modulated amide, polymer-based, HILICON AB), was used with H_2O containing 2 mM NH_4COOCH_3 and 2 mM $(NH_4)_2CO_3$ as MPA and ACN/MeOH (9/1, v/v) as MPB. The analytical measurements of the apolar fraction of the samples were carried out on an Agilent 1290 Infinity II LC system coupled to an Agilent 6560 DTIM-QToF-HRMS (Agilent Technologies, Santa Clara, USA) using Agilent Dual Jet Stream Electrospray Ionization.

In both ESI (+) and ESI (-) modes, an ACQUITY UPLC BEH C18 column (150 x 2.1 mm, 1.7 µm, Waters Corporation, Massachusetts, USA) was used with 5 mM NH_4COOCH_3 in H_2O/ACN (7/3, v/v) as MPA and 5 mM NH_4COOCH_3 in H_2O/ACN/IPA (2/10/88, v/v/v) as MPB. In ESI (+) mode, 0.1% (v/v) $HCOOCH_3$ was added to the aqueous fraction of MPA and MPB. Data were acquired in 2 GHz extended dynamic mode for all four analytical methods. Calibration of the mass axis was performed within run using purine (*m/z* 121.0508 in ESI (+) mode and *m/z* 119.0363 in ESI (-) mode) and hexakis (1H, 1H, 3H-tetrafluoropropoxy) phosphazine (*m/z* 922.0097 in ESI (+) mode and *m/z* 980.0163 in ESI (-) mode). The calibrant solution was constantly infused during the run with an additional isocratic pump. Details on the LC and QToF parameters can be found in SI (Table SI-2.1).

All samples were randomized before injection, and data were acquired in full scan (MS1) profile mode. A QC pooled sample was injected at regular intervals (n = 7). Data-dependent acquisition (auto-MS/MS) with iterative exclusion[20] was obtained during conditioning of the system by at least six injections of the QC pooled sample. Since lipids comprise a wide variety of isomers and isobars, additional ion mobility (IM) data was acquired for the QC pool of the apolar fraction of the HepaRG samples, both in single pulse and 4-bit multiplexed mode. Details on the drift tube (DT)IM parameters can be found in SI (Table SI-2.1).

2.6. LC-(DTIM)-HRMS data processing, pretreatment and statistics

Raw LC-HRMS data files (.d) were converted to .mzML format using MSConvert.[21] Subsequently, peak picking and alignment were performed in MS-DIAL (v. 4.6).[22] Details on used MS-DIAL parameters are provided in SI (Table SI-3.1). MS-FLO was used for additional deisotoping and removal of duplicates.[23] To evaluate the data quality, the relative standard deviation (RSD) of the intensity of each feature was plotted for each sample group separately. Intensity drift was corrected using cubic spline drift correction.[24] To avoid low-quality features, several filter steps were applied. Features present in at least 80% of sample

group C, H or L were retained. In addition, only features with an RSD < 30% in at least one exposure group were kept. For intracellular samples, features with maximum intensity lower than ten times the average intensity in the blank were removed. For extracellular samples, a fold change (FC) > 3 or < 0.33 between the average intensity in an exposure group and the average intensity in the blanks were used to retain a feature. In addition, features with maximal intensity in the QC pooled samples below 3000 were removed. Missing values were imputed using random forest (RF), and intensity values were log-transformed. Probabilistic quotient normalization (PQN) was performed using the median intensity of the QC pooled samples as a reference, followed by Pareto scaling.[24–26]

Principal component analysis (PCA) plots were built for visualization and removal of outliers. In addition, outlier samples were removed based on deviations in the detection of internal standards and/or a low number of features in a sample compared to other samples of the same group. Both univariate and multivariate statistics were applied because of their complementarity.[27] Before log transformation, normalization and scaling, a Shapiro-Wilk test was performed using the intensity values for each feature separately as a test of normality. Depending on the significance ($p < 0.05$) of the Shapiro-Wilk test, a Mann-Whitney U-test or a student-T-test was performed. Features with $p < 0.05$ and a FC > 5 or < 0.2 compared to sample group C, were considered significant. These high thresholds for the FC were used in order to retain only highly distinctive metabolites selected by univariate methods and to reduce the risk of selecting false positives due to a limited amount of cross-contamination of ethanol during incubation of control cells (see section 3.2).

Multivariate statistics included a binary RF classifier and partial least squares-discriminant analysis (PLS-DA) with 7-fold cross-validation. The PLS-DA model was evaluated by permutation of the y-variable (n = 1000) and by the R^2 and Q^2 value of the model, while the RF model was evaluated by the area under the curve (AUC). Interesting features were selected based on their variable importance in projection (VIP) value for the PLS-DA model and their mean decrease in accuracy or variable importance measure (VIM) for the RF model. Interesting features selected by the univariate or the multivariate model were only kept when they were selected both in the original experiments and the validation experiments. In addition, boxplots based on intensity of the features in each group were created for each selected feature and manually evaluated to decrease the number of false positives.

For the ion mobility data of the apolar fraction, multiplexed data files were de-multiplexed using the vendor-supplied software Agilent deMP. Data files were smoothed with a kernel size of 3 for drift and retention time and saturation repaired for points over 40% of the abundance limit using PNNL Preprocessor.[28] The collision cross-section ($^{DT}CCS_{N2}$) values were calculated using single-field calibration coefficients obtained by infusing the Agilent Tune Mix in IM-MS Browser B.08.00 (Agilent Technologies).

2.7. Annotation of metabolites of interest

For annotation of metabolites in the polar and apolar fractions, the All Public MS/MS library (v. 15) and the modified LipidBlast library were used for MS/MS matching in MS-DIAL (v. 4.6)[22], respectively, next to MS-Finder (v. 3.5)[29], MassBank[30], NIST library (v.17) with MS Search (v. 2.3, National Institute of Standards and Technology, Gaithersburg, MD, USA), METLIN[31], and GNPS[32] for both sample fractions. In addition, LipidMatch[33] and LipidHunter[34] were used to annotate features of the apolar fractions. Matched MS/MS spectra were manually evaluated to improve annotation confidence, and in-house standards were used for confirmation when available. Confirmation of fragments using rule-based fragmentation was used for manual evaluation of annotated lipids.[35,36] Only features that could be annotated with a level 3 (L3) confidence or higher, according to the annotation confidence system of Schymanski *et al*.[37], were considered. L3 refers to tentative candidates (i.e., insufficient information for one exact structure, e.g., annotation until lipid class level), while level 2 (L2) refers to a probable structure and is divided into 2a (i.e., unambiguous library spectrum match) and 2b (i.e., unambiguous annotation e.g., based on diagnostic MS/MS fragments, without available standard or literature for confirmation). Level 1 (L1) refers to a confirmed structure (i.e., confirmation using a reference standard with MS, MS/MS and RT matching). To further increase the annotation confidence for annotated lipids, CCS values were searched in experimental databases or *in silico* generated using AllCCS[38], when experimental values were unavailable, and annotated lipids were only considered when the CCS error was below 3%.[18]

3. RESULTS

3.1. IC_{10} determination

After exposure of HepaRG cells to eight different EtOH concentrations (range 250-950 mM, increments of 100 mM) for 24 h and 48 h (with renewal of EtOH-containing media after 24 h), cells were subjected to the neutral red uptake assay. Absorbance versus EtOH concentration was plotted using four-parameter logistics least squares regression (Fig. SI-4.1), which enabled the calculation of the IC_{50} and the Hill slope. The latter two parameters were used to calculate the IC_{10} value, according to equation 1.

$$IC10 = \left(\frac{90}{100-90}\right)^{1/H} * IC50$$

Equation 1. IC_{10} calculation using IC_{50} and Hill slope.

The IC_{10} value for HepaRG cells exposed for 24 h and 48 h to EtOH was determined to be 368 mM and 284 mM, respectively.

During exposure experiments, three sample groups (i.e. C, H and L) were obtained both for 24 h and 48 h of exposure. Post-exposure phase-contrast microscopic evaluation of the different sample groups was performed (Fig. 2). No clear morphological differences could be observed between cells of group C and

cells group L. However, when comparing group C to group H, for both time points, the polarized hepatocyte colonies show faded lining and impaired organization of hepatic clusters in addition to accumulated debris.

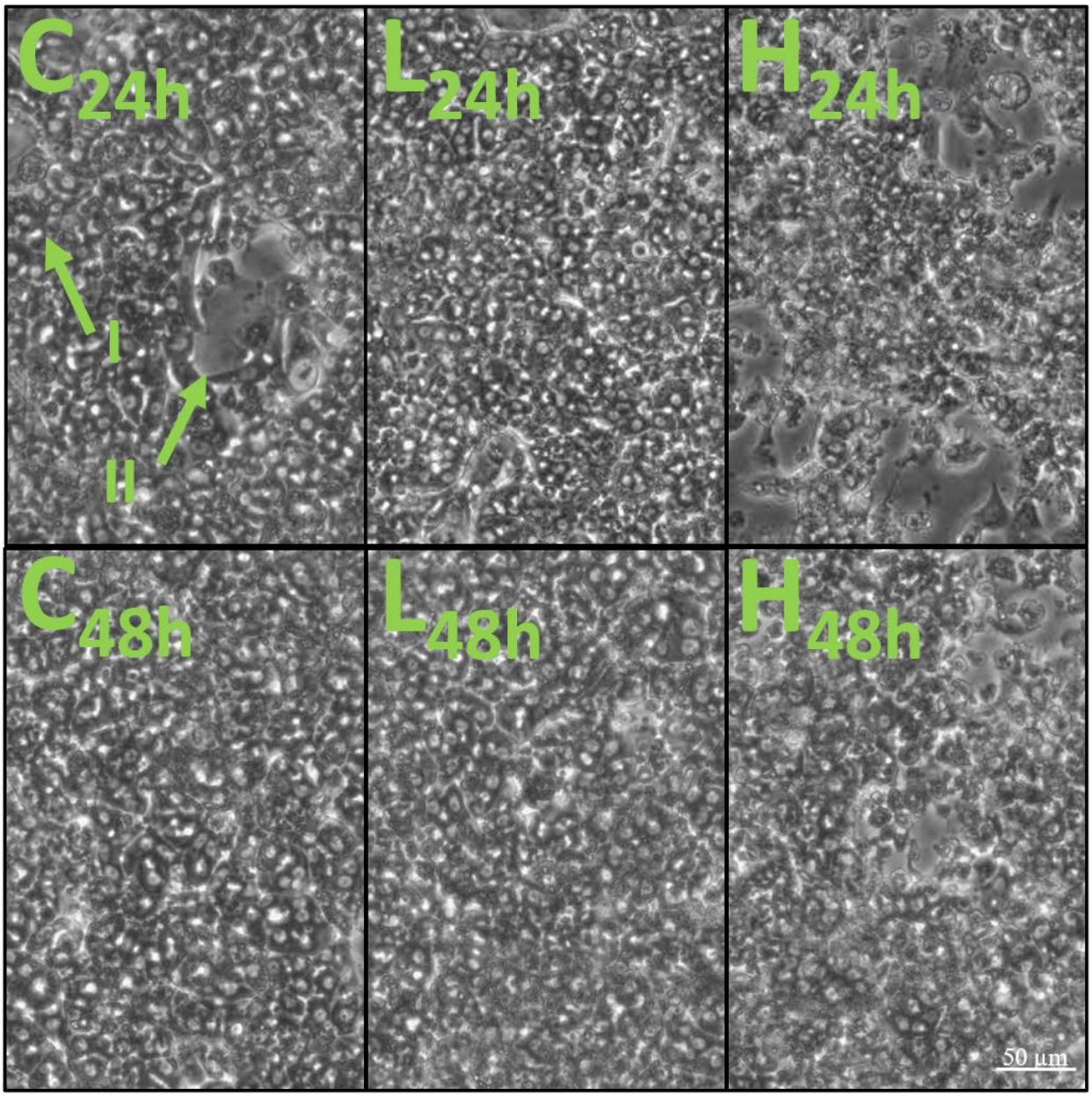

Fig. 2. Phase-contrast microscopic pictures of HepaRG cells (10x10). C_{24h}-L_{24h}-H_{24h}: control, 1/10 IC_{10} and IC_{10} after 24 h of exposure. C_{48h}-L_{48h}-H_{48h}: control, 1/10 IC_{10} and IC_{10} after 48 h of exposure. Roman numbers refer to polarized hepatocyte colonies (I) and biliary canaliculi and biliary-like epithelial cells (II).

3.2. HS-GC-FID analyses

During exposure experiments, different sample groups were exposed to five different concentrations of ethanol (i.e., 368 mM – $IC_{10\text{-}24h}$, 284 mM – $IC_{10\text{-}48h}$, 36.8 mM – 1/10 $IC_{10\text{-}24h}$, 28.4 mM – 1/10 $IC_{10\text{-}48h}$, and 0 mM – control). The ethanol content of the media was determined post-incubation using HS-GC-FID. Results are presented in Fig. 3. Incubation for 24 h caused an average decrease in ethanol concentration of 50% for the IC_{10} and 39% for 1/10 of the IC_{10}. Incubation for 48 h with renewal of ethanol containing media after 24 h showed a decrease of 48% for the IC_{10} and 34% for 1/10 of the IC_{10}. After 24 h and 48 h, control samples showed an ethanol content of 1.1% and 1.4% compared to the IC_{10}, respectively. Pre- and post-run ethanol QC solutions were quantified both as 0.3 g/L for the 0.3 g/L solution and 3.9 g/L and 4.0 g/L for the 4.0 g/L solution, respectively. The monitoring of cross-contamination due to ethanol evaporation is important as complete avoidance of cross-contamination would only be possible when using closed systems to incubate cells, which would not allow necessary gas exchange, or when using separate incubators for each concentration. This latter would require a lab environment equipped with a dedicated incubator for each ethanol concentration and can increase non-biological inter-group variation due to variance in temperature, $\%CO_2$ and humidity between incubators.

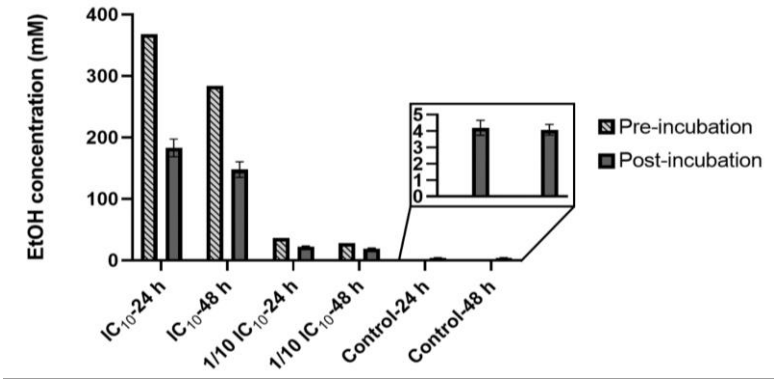

Fig. 3. Reduction of ethanol concentration during incubation. Headspace gas chromatography with flame ionization detection (HS-GC-FID) was used to determine the ethanol concentration pre-incubation (n = 1) and post-incubation (n = 6).

3.3. Data quality

Post-run quality control included manual evaluation of extracted ion chromatograms of internal standards. Pre-set requirements for data quality of internal standards needed to be fulfilled for retaining a sample and included mass error < 10 ppm, RT deviation < 0.5 min for HILIC-HRMS and 0.2 min for RPLC-HRMS. For the intracellular samples, mRSDs were < 15% for all QC samples of the apolar fraction and < 20% for all QC samples of the polar fractions, with one exception (21% for ESI (+) after 24 h exposure – batch 1) (Table SI-5.1). Concordant with the intracellular fraction, mRSDs of the QC samples of the apolar fraction

of the extracellular samples (Table SI-5.2) were all < 15%. While the mRSDs of the QC samples of the polar fraction in positive ionization modes were < 15%, higher mRSDs were seen for the polar fraction in negative ionization mode, with an average mRSD of 22%. All calculated mRSD values indicate a reliable analytical method as RSD values ≤ 30% are generally accepted in untargeted metabolomics.[39] Biological and sample preparation variance is indicated by the increase in mRSD between QC samples and biological samples (i.e., sample groups C, H and L). For the intracellular samples, the average mRSD increased from 12% to 23% and from 16% to 23% for the apolar and polar fractions, respectively. The increase in average mRSD was slightly lower for the extracellular samples, with 11% to 20% for the apolar fractions and 17% to 20% for the polar fractions. The low increase in mRSD indicates little sample preparation and biological variance.

Principal component analysis (PCA) plots (Fig. SI-5.1-SI-5.8) showed a clear separation in PC1 and/or PC2 between sample group H and the other sample groups indicating a high inter-group variability due to a strong metabolic impact of ethanol exposure. For example, the PCA plot of the apolar fraction of the intracellular samples of HepaRG cells exposed to ethanol for 24 h, in ESI (+) mode, is shown in Fig. 4.

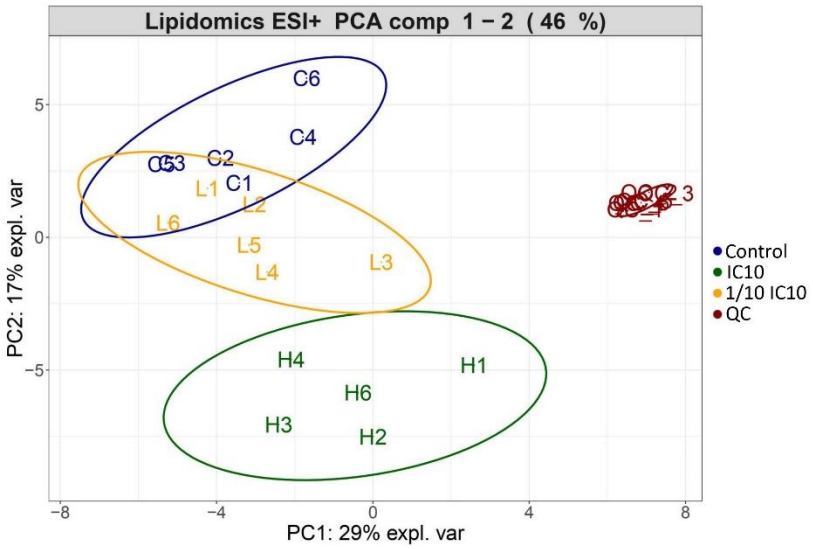

Fig. 4. Example of a principal component analysis plot of the apolar fraction of intracellular samples of HepaRG cells analyzed in ESI (+) mode, after 24 h exposure to ethanol. There is a clear distinction between the control group (C, blue) and the sample group exposed to the IC_{10} of ethanol (H, green), while there is a slight overlap between the control group and the sample group exposed to 1/10 of the IC_{10} of ethanol (L, orange). This latter indicates a larger metabolic difference between control – IC_{10} compared to control – 1/10 IC_{10}. The clustering of pooled QC samples is shown in red.

For 24 h and 48 h exposure, inter-group variability between group C and group L was often insufficient to obtain a clear separation in PC1 and PC2. The higher similarity in metabolic profile can explain the overlap between these two groups. The degree of overlap between group C and L depended on the analyzed fraction, reflected by a higher overlap for the apolar fractions and a better separation for the polar fractions. There is a clear distinction between group C and L in PC1 and/or PC2 in ESI (+) mode, while more overlap is seen in ESI (-) mode.

In line with the trends observed during the PCA analysis, the evaluation parameters of the multivariate statistical models (i.e., R^2, Q^2, R^2_{PERM}, Q^2_{PERM} (n permutations = 1000) for the PLS-DA models and AUC for the RF models, Table SI-5.3-SI-5.6), high values were found for R^2 ($\bar{x}_{IC}$ = 0.95, $\bar{x}_{EC}$ = 0.95), Q^2 ($\bar{x}_{IC}$ = 0.83, $\bar{x}_{EC}$ = 0.86), and AUC ($\bar{x}_{IC}$ = 0.99, $\bar{x}_{EC}$ = 0.99) and low values for R^2_{PERM} ($\bar{x}_{IC}$ = 0.01, $\bar{x}_{EC}$ = 0.02) and Q^2_{PERM} ($\bar{x}_{IC}$ = 0.01, $\bar{x}_{EC}$ = 0.00) for the models comparing the group C with H. PLS-DA and RF models comparing the group C with L showed lower values for R^2 ($\bar{x}_{IC}$ = 0.92, $\bar{x}_{EC}$ = 0.85), Q^2 ($\bar{x}_{IC}$ = 0.55, $\bar{x}_{EC}$ = 0.52), and AUC ($\bar{x}_{IC}$ = 0.76, $\bar{x}_{EC}$ = 0.82) and higher values for R^2_{PERM} ($\bar{x}_{IC}$ = 0.31, $\bar{x}_{EC}$ = 0.20) and Q^2_{PERM} ($\bar{x}_{IC}$ = 0.18, $\bar{x}_{EC}$ = 0.09).

3.4. Metabolomic fingerprint of ethanol-induced hepatotoxicity in HepaRG cells

Features selected by univariate (Mann-Whitney U-test or a student-T-test combined with FC cut-off) and/or multivariate statistical approaches (PLS-DA and RF) were only kept for annotation when selected in both the exposure experiment and the validation experiment. Annotated metabolites with their observed RT, *m/z* value, $^{DT}CCS_{N2}$ value and additional information are listed in Table SI-6.1. The effect of ethanol exposure on the intracellular metabolome of HepaRG cells is shown in Fig. 5.

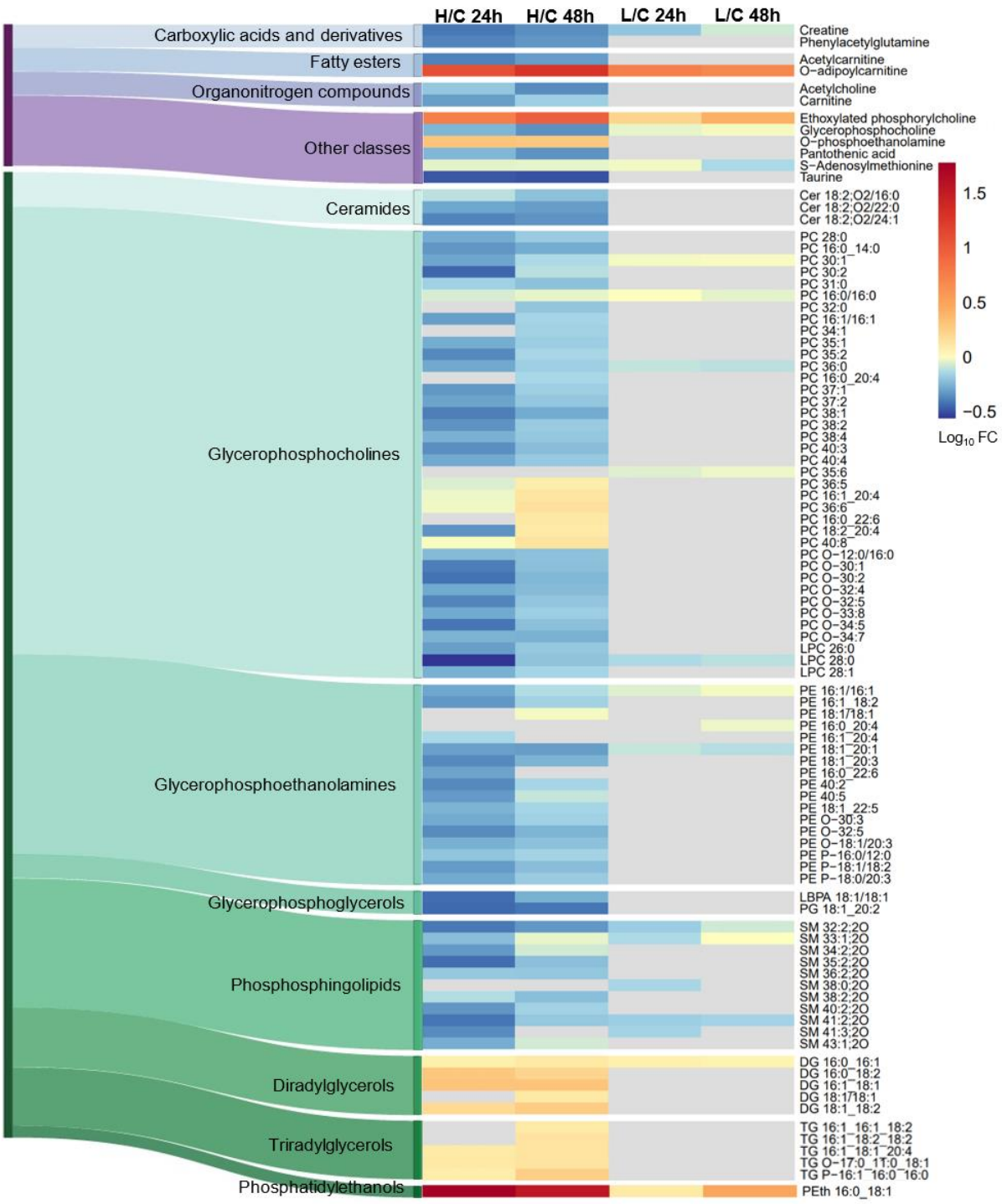

Fig. 5. Sankey diagram combined with heatmaps to show the effect of ethanol exposure on the intracellular metabolome of HepaRG cells. Only annotated metabolites selected by univariate and/or multivariate statistics are shown. Altered metabolites in the polar fraction of the samples are indicated by a blue-purple Sankey diagram, while a green Sankey diagram represents metabolites originating from the apolar fraction. Grey color in the heatmap was used when a metabolite was not selected during the statistical selection. H/C

24 h: IC_{10} vs control after 24 h of ethanol exposure. H/C 48 h: IC_{10} vs control after 48 h of ethanol exposure. L/C 24 h: 1/10 IC_{10} vs control after 24 h of ethanol exposure. L/C 48 h: 1/10 IC_{10} vs control after 48 h of ethanol exposure. FC: fold change.

In total, 94 altered metabolites selected during the statistical workflow could be annotated. Of the 82 lipids, 40 were annotated as L2 and 42 as L3, while of the 12 polar metabolites, 8 were annotated as L1 and 4 as L2. Annotation levels and libraries used for MS/MS matching per metabolite can be consulted in the supplementary spreadsheet. Usage of multiple libraries is recommended as their combination increases coverage. For example, 77% of annotated lipids were elucidated using the modified LipidBlast library of MS-DIAL (v. 4.6), while 49% and 25% of lipids were annotated using LipidMatch and LipidHunter respectively. The lower coverage of LipidHunter can be explained by the limited number of selectable ionization species. For polar metabolites, NIST (v. 17) and MassBank yielded the highest coverage (both 92%), followed by METLIN (69%), GNPS (61%), the All Public MS/MS library (v. 15) of MS-DIAL (54%) and MS-Finder (38%).

As expected, based on the results of the PCA analysis and the evaluation parameters of the PLS-DA and RF models, a more distinct metabolic pattern is observed after ethanol exposure at the IC_{10} than at 1/10 of the IC_{10}. In group H, upregulation was observed during 24 h and 48 h exposure for diacylglycerols (DG) and triacylglycerols (TG), with more TGs upregulated after 48 h exposure. At both time points, a downregulation was observed for ceramides with a d18:2 backbone (Cer d18:2), lysophosphatidylcholines (LPC), phosphatidylcholines (PC), phosphatidylethanolamines (PE) and sphingomyelines (SM). Interestingly, polyunsaturated PCs ($\geq$ 5 double bonds) were slightly upregulated after 48 h exposure, while they were downregulated after 24 h exposure. In addition, two glycerophosphoglycerols (LBPA 18:1/18:1 and PG 18:1_20:2) were downregulated. PEth 16:0_18:1, as a marker of ethanol exposure, was detected at high intensity in all exposed samples.

Concerning polar metabolites, there was a downregulation of acetylcholine, creatine, glycerophosphocholine, pantothenic acid, phenylacetylglutamine, S-adenosylmethionine (SAM) and taurine. Upregulation was observed for O-phosphoethanolamine. While short-chain acylcarnitines (< C5) were downregulated, O-adipoylcarnitine, a medium-chain acylcarnitine (C6-C13), was strongly upregulated. Similar up- and downregulations were observed for group L during 24 h and 48 h exposure (Fig. 5); although fewer metabolic classes were affected, fold changes were lower and affected classes were represented by a lower number of species. Ethoxylated phosphorylcholine was found highly upregulated in each exposure group. The high fold change was caused by its absence in the group C. Since no MS/MS library could be found for this latter metabolite, its fragmentation was matched using NIST (v.17) without accurate *m/z* matching, enabling fragmentation spectral matching with fragments of other metabolites with

a higher *m/z* value. In addition, the fragmentation spectra of ethoxylated phosphorylcholine were confirmed with *in silico* generated fragments using CFM-ID (v. 4.0)[40] (Fig. SI-8.1-SI-8.3).

3.5. Metabolomic footprint of ethanol-induced hepatotoxicity in HepaRG cells

As for elucidation of the metabolomic fingerprint, features were selected by univariate and/or multivariate statistics and were only kept for annotation when selected in both the exposure and validation experiments. Annotated metabolites with their observed RT, *m/z* value, $^{DT}CCS_{N2}$ value and additional information are listed in Table SI-7.1. The effect of ethanol exposure on the extracellular metabolome of HepaRG cells is shown in Fig. 6. The lower number of selected features in the extracellular fraction (Fig. 6 shows 23 altered metabolites) compared to the intracellular fraction (Fig. 5 shows 94 altered metabolites) can be explained by the complex extracellular matrix as incubation media contained calf serum among various other components. Of the 11 lipids, 1 was annotated as L1 and 10 as L2, while of the 12 polar metabolites, 4 were annotated as L1 and 8 as L2. Annotation levels and libraries used for MS/MS matching per metabolite can be consulted in the supplementary spreadsheet. From the annotated lipids, 71% could be elucidated using LipidMatch, 50% using the modified LipidBlast library of MS-DIAL (v. 4.6) and 21% using LipidHunter. For polar metabolites, the highest coverage was yielded by NIST (v. 17) (83%), followed by MassBank (67%), GNPS (58%), MS-Finder (50%), METLIN (42%) and the All Public MS/MS library (v. 15) of MS-DIAL (33%).

When comparing exposure vs control samples for metabolomic footprinting, it is challenging to assign up- or downregulation to either changes in hepatic metabolite secretion or to changes in consumption of media components.

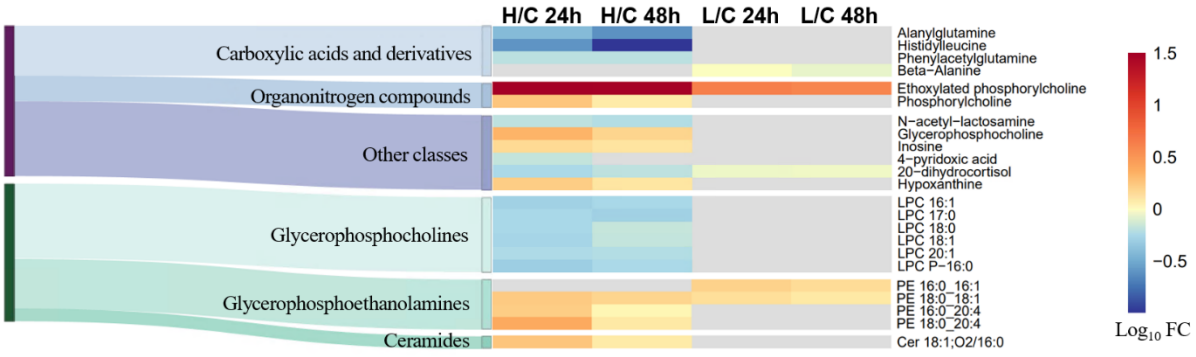

Fig. 6. Sankey diagram combined with heatmaps to show the effect of ethanol exposure on the extracellular metabolome of HepaRG cells. Only annotated metabolites selected by univariate and/or multivariate statistics are shown. Altered metabolites in the polar fraction of the samples are indicated by a blue-purple Sankey diagram, while a green Sankey diagram represents metabolites originating from the apolar fraction.

Grey color in the heatmap was used when a metabolite was not selected during the statistical selection. H/C 24 h: IC_{10} vs control after 24 h of ethanol exposure. H/C 48 h: IC_{10} vs control after 48 h of ethanol exposure. L/C 24 h: 1/10 IC_{10} vs control after 24 h of ethanol exposure. L/C 48 h: 1/10 IC_{10} vs control after 48 h of ethanol exposure. FC: fold change.

In order to be able to distinguish altered secretion from altered consumption, Fig. SI-7.1 was included in the supplementary information. This figure shows the fold change differences between (I) exposure vs control, (II) exposure vs blank media and (III) control vs blank media, with blank media referring to extraction blanks (i.e., incubated media without cells). A negative fold change for all three groups indicates metabolites that show an increased consumption during ethanol exposure, while a positive fold change for all groups indicates an increased secretion. Metabolites downregulated in group (II) and (III) and upregulated in group (I), indicate metabolites that are less consumed by HepaRG cells. A fourth scenario is upregulation in group (II) and (III) and downregulation in group (I), indicating reduced secretion. As metabolomic studies provide a snapshot of metabolic patterns, the four described scenarios should be interpreted carefully since changes can be highly dynamic.

For group H after 24 h and 48 h exposure, increased secretion was observed for PEs and Cer 18:1;O2/16:0, while LPCs were downregulated because of higher consumption. Concerning polar metabolites, there was a downregulation of N-acetyl-lactosamine, phenylacetylglutamine and 4-pyridoxic acid (only after 48 h exposure), due to a decreased secretion. Alanylglutamine and histidylleucine were downregulated due to higher consumption. Glycerophosphocholine, hypoxanthine and inosine were upregulated because of lower consumption, while phosphorylcholine was upregulated due to increased secretion. Metabolic changes in sample group L were less profound compared to group H, with only upregulation of PEs in the apolar sample fraction. Beta-alanine was downregulated due to less secretion only in group L. 20-dihydrocortisol was less secreted in all exposure groups. Interestingly, high secretion of ethoxylated phosphorylcholine was found in each exposure group.

4. DISCUSSION

An overview of the most important metabolic changes due to ethanol exposure in HepaRG cells is presented in Fig. 7.

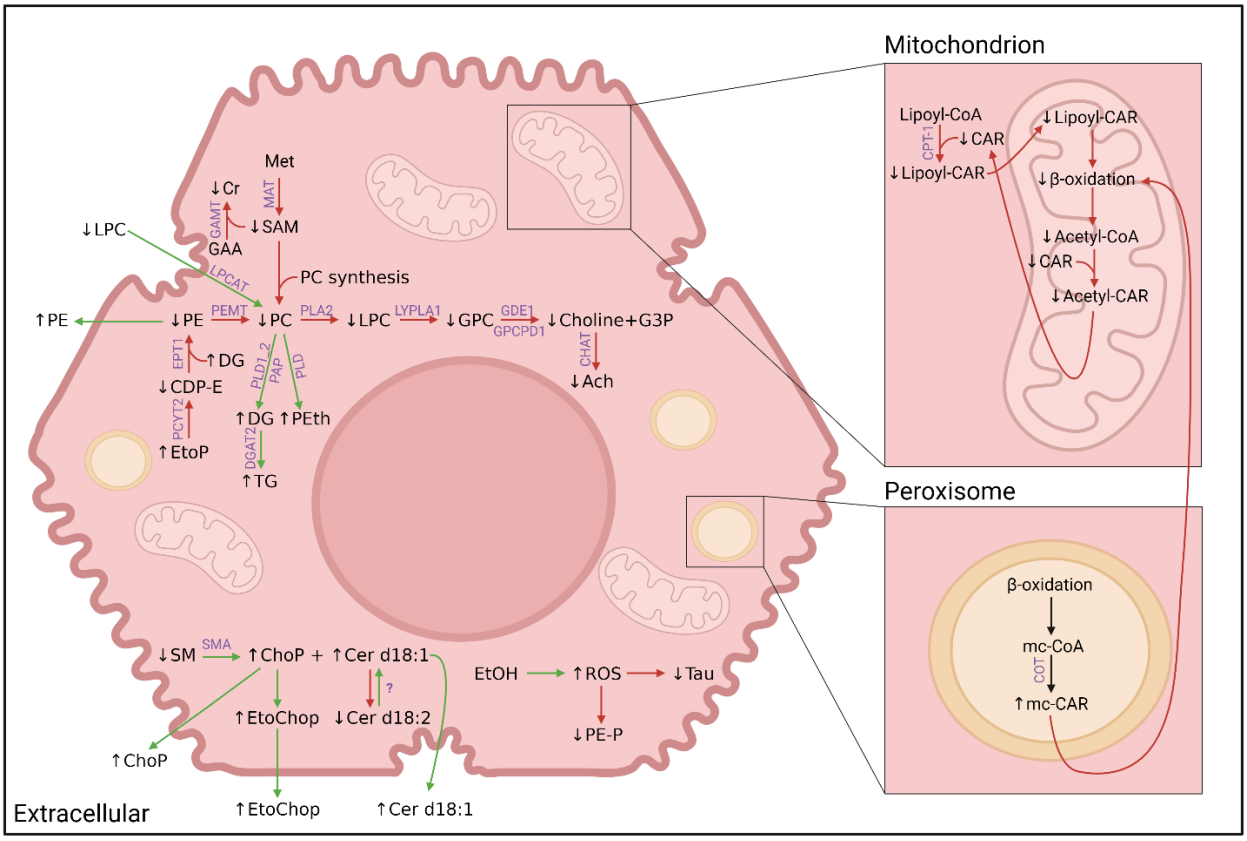

Fig. 7. Metabolic changes in HepaRG cells after ethanol exposure. Intracellular green and red arrows were used to indicate increased and decreased biosynthesis/availability, respectively. Green arrows connecting the intracellular and extracellular compartment indicate increased secretion or uptake, depending on their direction. Ach: Acetylcholine. CAR: Carnitine. CDP-E: CDP-ethanolamine. Cer: Ceramide. CHAT: Choline O-acetyltransferase. ChoP: Posphorylcholine. CoA: Coenzyme A. COT: Carnitine octanoyltransferase. CPT-1: Carnitine palmitoyltransferase 1. Cr: Creatine. DG: Diglyceride. DGAT2: Diglyceride acyltransferase 2. EPT1: Ethanolaminephosphotransferase 1. EtOChoP: Ethoxylated phosphorylcholine. EtoP: O-phosphoethanolamine. G3P: Glycerol 3-phosphate. GAA: Guanidinoacetate. GAMT: Guanidinoacetate methyltransferase. GDE1: Glycerophosphodiester phosphodiesterase 1. GPC: Glycerophosphocholine. GPCPD1: Glycerophosphocholine phosphodiesterase 1. LPC: Lysophosphatidylcholine. LPCAT: Lysophosphatidylcholine acyltransferase. LYPLA1: Lysophospholipase 1. MAT: Methionine adenosyltransferase. mc-CAR: medium chain-CAR. mc-COA: medium chain-CoA. Met: Methionine. PAP: Phosphatidate phosphatase. PC: Phosphatidylcholine. PCYT2 : Phosphoethanolamine cytidylyltransferase. PE: Phosphatidylethanolamine. PEMT: Phosphatidylethanolamine-N-methyltransferase. PE-P: Alkenyl ether phosphatidylethanolamine. PEth: Phosphatidylethanol. PLA2: Phospholipase A2. PLD: Phospholipase D. PLD1_2: Phospholipase D1/2.

ROS: Reactive oxygen species. SAM: S-adenosyl methionine. SM: Sphingomyeline. SMA: Sphingomyelinase. Tau: Taurine. TG: Triglyceride.

4.1. PCs and their relation to PEs, DGs, TGs, PEth and SAM

It is known that ethanol exposure inhibits phosphatidylethanolamine-N-methyltransferase (PEMT), causing a lower production rate of PCs from PEs.[41] In addition, the accumulation of PEth reduces the PC content since PEth is formed by the exchange of ethanol for choline in PCs. PEth is a phospholipid only formed in the presence of ethanol in a reaction catalyzed by phospholipase D (PLD). Previously, hepatic PEth accumulation has been shown *in vivo* and *in vitro*.[42,43] A third effect that can explain the downregulation of hepatic PCs is the ethanol-induced reduction of SAM formation by the inhibition of methionine synthase and methionine adenosyltransferase, which disturbs hepatic methyl transfer necessary for the generation of PCs.[41,44] In addition, SAM reduction could explain the downregulation of intracellular creatine, as its hepatic synthesis is catalyzed by guanidinoacetate methyltransferase (GAMT), which uses SAM as a methyl donor.[45] A fourth mechanism explaining decreased hepatic PC content is the shift towards TG synthesis through initial conversion of PCs to DGs, supported by the finding of upregulation of DG acyltransferase 2 (DGAT2) after ethanol consumption by mice.[46] The increase in DGs and TGs can additionally be explained by the ethanol-induced upregulation of lipin-1, which is considered a key enzyme in the pathogenesis of ALD and shows a dual function as phosphatidic acid phosphohydrolase enzyme and transcriptional coregulator.[47,48] The general image showed a decrease of PCs in the intracellular fraction of HepaRGs after 24 h and 48 h of ethanol exposure. However, after 48 h, a slight increase of highly unsaturated PCs (≥ 5 double bonds) was observed. This might relate to the shift of saturated to unsaturated fatty acids as observed in alcohol-fed rodents.[49] Polyunsaturated fatty acids can be incorporated in DGs and subsequently in PCs through the CDP-choline pathway.[49]

4.2. LPCs and GPC

In addition to decreased hepatic PCs, a similar trend was observed for hepatic LPCs. Israelsen *et al.* observed a decrease of LPCs in human hepatic venous blood after alcohol intoxication in healthy volunteers and ALD patients, with only minor effects in patients suffering from non-alcoholic fatty liver disease (NAFLD).[50] These results are concordant with the reduction of LPCs caused by increased consumption in the extracellular fraction of HepaRG cells exposed to ethanol. The authors hypothesized that the reduction of circulating LPCs could be caused by an increased hepatic uptake, which was confirmed in this study. However, our results show a decreased level of LPCs, both in the intracellular and extracellular fractions. The decrease of intracellular LPCs is in agreement with the findings of Puri *et al.* and Koelmel *et al.*, who reported a decreased hepatic LPC content in mice which were fed a diet rich in ethanol.[51,52] Puri *et al.* found

that the decrease in hepatic LPCs was more pronounced in obese than lean mice. Additionally, Puri *et al.* saw an insignificant decrease in hepatic LPCs in human patients suffering from NAFLD, while they were significantly increased in non-alcoholic steatohepatitis (NASH), suggesting an important inflammatory component for LPC upregulation, which could contribute to lipoapoptosis of hepatocytes.[53,54] Stefanescu *et al.* suggested prognostic importance of LPC decrease in the serum of patients with ALD.[55] The downregulation of PCs due to a shift towards TG synthesis amongst others, could explain the reduced catabolism of PCs by deacylation to LPCs catalyzed by phospholipase A2 (PLA2). This hypothesis is supported by the intracellular decrease of glycerophosphocholine (GPC), the deacylation product of LPCs, formed in the second step of PC catabolism, catalyzed by lysophospholipase I (LYPLA1). Increased uptake of LPCs from the extracellular environment might be used to fuel the formation of GPC by LYPLA1 and/or to fuel the PC pool by lysophosphatidylcholine acyltransferase (LPCAT). Downregulation of GPC facilitates the observed intracellular reduction of acetylcholine, as GPC, formed during PC catabolism, can be converted into glycerol-3-phosphate and free choline, available for the biosynthesis of acetylcholine.[56]

4.3. PEs and their relation to DGs, TGs and EtoP

Despite ethanol-induced inhibition of PEMT, a decrease in hepatic PEs was seen in intracellular HepaRG extracts. This is consistent with the significant decrease of hepatic PEs observed in human patients suffering from NAFLD and the decrease of PEs in HepaRG cells after steatosis induction using sodium valproate.[53,57] An impaired activity of phosphoethanolamine cytidylyltransferase (PCYT2) in the CDP-ethanolamine pathway might explain the decreased content of PEs. Impaired activity of the latter enzyme would also contribute to the accumulation of hepatic O-phosphoethanolamine (EtoP) and DGs, which are normally used for the synthesis of CDP-ethanolamine. In addition, accumulated DGs can be used for the synthesis of TGs, increasing the steatotic image.[58] In PCYT2 knockout mice, deletion of the PCYT2 allele caused the development of liver steatosis.[59] However, the hypothesis of impaired activity of phosphoethanolamine cytidylyltransferase does not explain the increase in extracellular PEs and could not be confirmed since the effect of ethanol exposure on this enzyme has not been studied. Another possibility is that the decrease in intracellular PEs and the increase in extracellular PEs are related to the altered secretion of PEs in VLDL-type chylomicrons.[57] Dysregulation of phospholipid synthesis in hepatocytes, observed as deviations of PC and PE abundances and the molar ratio of PC/PE can affect cell membrane integrity, assembly and secretion of VLDL and mitochondrial bioenergetics.[60,61]

4.4. Ether lipids and taurine

In addition to decreased hepatic PCs and PEs, ether lipids (e.g., ether-PC and ether-PE) were decreased in the intracellular fraction. This latter relates to both alkyl and alkenyl ether glycerophospholipids. Alkenyl

ether lipids are important antioxidants, and the decrease could be explained by their involvement during the clearance of reactive oxygen species (ROS) generated during ethanol metabolism.[62] Although the understanding of the function of ether lipids is growing, there are still large knowledge gaps, especially in relation to pathophysiology.[63] In addition to ether lipids, the intracellular decrease of taurine could also be related to the clearance of ROS, as Wu *et al.* demonstrated that taurine administration increased hepatic antioxidant capacity and reduced lipid peroxidation in ethanol-fed rats.[64]

4.5. SMs and their relation to Cers and ChoP

The decrease of hepatic SMs is in accordance with the previously observed downregulation of SMs in human serum of heavy drinkers, which could be due to increased hydrolysis of SMs into Cers and phosphorylcholine (ChoP) by sphingomyelinase (SMA).[42] This decrease of SMs and increased activity of sphingomyelinase was also observed in ethanol-exposed HepG2 cells.[65] In studies describing upregulation of hepatic Cers after ethanol exposure, Cers with a sphing-4-enine-backbone (d18:1) are listed, which could contribute to blocking fatty acid oxidation and promote its synthesis by inhibition of the phosphorylation of adenosine monophosphate-activated protein kinase (AMPK).[66,67] During the present study, no increased hepatic Cer d18:1 species could be annotated after statistical selection, possibly because the FC differences were not large enough. However, three selected Cers with a sphingadienine-backbone (d18:2) were downregulated (FC between 0.4 and 0.7). Since data on Cer d18:2 species and their biological relevance is limited, an example MS/MS spectrum for Cer 18:2;O2/22:0 was included (Fig. SI-8.5). Both Cer d18:1 species and phosphorylcholine were upregulated in the extracellular fraction due to increased secretion.

4.6. CARs and vitamins

As steatosis can impair hepatic biosynthesis of L-carnitine, which is necessary for the transfer of long-chain fatty acids to mitochondria, subsequent β-oxidation is reduced, leading to toxic cytoplasmatic accumulation of fatty acids.[68,69] In addition, ethanol inhibits carnitine palmitoyltransferase 1 (CPT-1) activity, a rate-limiting step in fatty acid translocation for mitochondrial β-oxidation.[70] Under physiological conditions, carnitine can buffer excess acetyl-CoA in the mitochondria via the formation of acetyl-carnitine for mitochondrial export by carnitine acylcarnitine translocase.[69] The reduction of acetyl-carnitine in the intracellular extracts after ethanol exposure of HepaRG cells can be explained by the impaired β-oxidation, reducing the biosynthesis of acetyl-CoA in mitochondria. Another possible contributing factor is the intracellular reduction of pantothenic acid, one of the precursors of CoA, which was also observed in the liver of ethanol-fed rats.[71–73] Next to a decrease of hepatic pantothenic acid in ethanol-fed rats, Miyazaki *et al.* targeted different B-group vitamins and observed a decreased excretion of 4-pyridoxic acid, a catabolite of vitamin B6. This result is concordant with the decreased hepatic secretion of 4-pyridoxic acid in HepaRG

cells after 48 h of ethanol exposure. The authors hypothesized increased hepatic storage of vitamin B6 during ethanol exposure.[72]

Since acetyl-carnitine can provide acetyl groups for the production of acetylcholine catalyzed by choline acetyltransferase, the reduction of acetyl-carnitine facilitated downregulation of hepatic acetylcholine, which is also in line with the reduced uptake of extracellular GCP. However, as cytosolic acetyl-CoA can also be used as acetyl source, there is a strong likelihood for additional mechanisms of acetylcholine reduction.[74] The strong intracellular upregulation of octanoyl-carnitine could also be explained by impaired β-oxidation. Very long-chain and branched-chain fatty acids are mainly oxidized in peroxisomes, while long-chain fatty acid are β-oxidized both in peroxisomes and mitochondria. As peroxisomal oxidation of fatty acids is incomplete, shortened medium-chain acyl-CoAs are generated that need to be transported to mitochondria for further oxidation. As the generated medium-chain acyl-CoAs are membrane-impermeable, they are converted to their respective carnitine esters by peroxisomal carnitine octanoyltransferase (COT) for transportation out of peroxisomes.[75]

4.7. 20-dihydrocortisol

Decreased hepatic secretion of 20-dihydrocortisol could be explained by decreased expression of AKR1D1. This latter gene encodes 3-oxo-5-beta-steroid 4-dehydrogenase, which is responsible for catalyzing the conversion of cortisol to 20-dihydrocortisol. In human liver biopsies from NAFLD patients, a decrease of AKR1D1 expression was observed with advancing steatosis, fibrosis and inflammation and a relation with triglyceride accumulation and reduced beta-oxidation amongst others, was observed using human liver cell lines with AKR1D1 knockdown by Nikolaos *et al.*[76]

4.8. Ethoxylated phosphorylcholine

Ethoxylated phosphorylcholine (Fig. SI-8.1-SI-8.4), a previously unreported metabolite, might be a new marker of ethanol exposure. Due to its absence in the control samples, the metabolite showed similar large fold changes to PEth 16:0_18:1. Interestingly, unlike PEth 16:0_18:1, ethoxylated phosphorylcholine was found both in intracellular and extracellular samples due to a high level of hepatic secretion.

5. CONCLUSIONS

HepaRG cells are considered as an appropriate surrogate for primary human hepatocytes when investigating liver metabolism and detoxification[77], while untargeted metabolomics can be used to generate pathophysiological hypotheses and could pinpoint etiology-dependent metabolic differences in liver disease. Combining the elucidation of the metabolic fingerprint and footprint of ethanol-induced hepatotoxicity in HepaRG cells facilitated the biological interpretation of results. Metabolic alterations

showed only minor differences between 24 h and 48 h of exposure, with more upregulated TGs with a high level of confirmation and more polyunsaturated PCs after 48 h of exposure. However, metabolic alterations were strongly affected by the exposure concentration of ethanol. Many altered metabolites were consistent with a steatotic image as seen in previous research, such as increased intracellular DGs and TGs, phosphorylcholine and Cers (d18:1), decreased PEs, PCs, LPCs, SMs, SAM and small chain CARs. Additional markers of toxicity have been observed such as downregulation of Cers (d18:2), creatine, O-phosphoethanolamine and acetylcholine and upregulation of octanoylcarnitine. Decreased catabolism of PCs to LPCs was supported by the decrease in GPC. In addition to detection of high levels of intracellular PEth 16:0_18:1, ethoxylated phosphorylcholine could be identified, both intra- and extracellular. Based on its absence in control samples, ethoxylated phosphorylcholine could be considered as a potential new marker of ethanol exposure, although *in vivo* confirmation and further validation would be required.

DATA AVAILABILITY STATEMENT

Raw datafiles are available through the MassIVE repository (https://massive.ucsd.edu/ProteoSAFe/) with the data set identifier MSV000088638.

NOTES

The authors declare no competing financial interest.

ASSOCIATED CONTENT

Supporting Information.

Section 1. Sample preparation of HepaRG cells

SI-1.1 Sample preparation of intracellular HepaRG extracts

SI-1.2 Sample preparation of extracellular HepaRG extracts

SI-1.3 Optimization of dilution factor for extracellular HepaRG extracts

Figure SI-1.3.1 Dilution series used during optimization of the dilution factor for the extracellular fraction of HepaRG sample extracts

Figure SI-1.3.2 Mean intensity of features in relation to the dilution factor of the extracellular apolar and polar fraction of HepaRG cells

Section 2. Data acquisition

Table SI-2.1 Data acquisition parameters per sample fraction

Section 3. MS-DIAL parameters

ACKNOWLEDGMENTS

Elias Iturrospe acknowledges funding of the Research Scientific Foundation-Flanders (FWO) - project number 1161620N. Katyeny Manuela da Silva, Rani Robeyns and Maria van de Lavoir are funded by the University of Antwerp (BOF DOCPRO 4 - Antigoon ID 36893, BOF-GOA – PS ID 41667 and BOF – Antigoon ID 46315, respectively). Graphical icons in Fig. 1 and Fig. 7 were provided by BioRender, license n. 2641-5211. Fig. 3 was made using Graphpad Prism (v. 9.0). Further funding of this research has been provided by the University of Antwerp (UA, Belgium) and the Vrije Universiteit Brussel (VUB, Belgium).

REFERENCES

(1) Asrani, S. K.; Devarbhavi, H.; Eaton, J.; Kamath, P. S. Burden of Liver Diseases in the World. *J. Hepatol.* **2019**, *70* (1), 151–171. https://doi.org/10.1016/J.JHEP.2018.09.014.

(2) Sakhuja, P. Pathology of Alcoholic Liver Disease, Can It Be Differentiated from Nonalcoholic Steatohepatitis? *World J. Gastroenterol.* **2014**, *20* (44), 16474–16479. https://doi.org/10.3748/WJG.V20.I44.16474.

(3) Seitz, H. K.; Bataller, R.; Cortez-Pinto, H.; Gao, B.; Gual, A.; Lackner, C.; Mathurin, P.; Mueller, S.; Szabo, G.; Tsukamoto, H. Alcoholic Liver Disease. *Nat. Rev. Dis. Prim.* **2018**, *4* (1), 16. https://doi.org/10.1038/S41572-018-0014-7.

(4) World Health Organization. *Global Status Report on Alcohol and Health 2018*; Geneva, 2018.

(5) Chacko, K. R.; Reinus, J. Spectrum of Alcoholic Liver Disease. *Clin. Liver Dis.* **2016**, *20* (3), 419–427. https://doi.org/10.1016/J.CLD.2016.02.002.

(6) Liangpunsakul, S.; Haber, P.; McCaughan, G. W. Alcoholic Liver Disease in Asia, Europe, and North America. *Gastroenterology* **2016**, *150* (8), 1786–1797. https://doi.org/10.1053/J.GASTRO.2016.02.043.

(7) Sheron, N.; Moore, M.; O'Brien, W.; Harris, S.; Roderick, P. Feasibility of Detection and Intervention for Alcohol-Related Liver Disease in the Community: The Alcohol and Liver Disease Detection Study (ALDDeS). *Br. J. Gen. Pract.* **2013**, *63* (615), e698–e705. https://doi.org/10.3399/BJGP13X673711.

(8) European Association for the Study of the Liver. EASL Clinical Practice Guidelines: Management of Alcohol-Related Liver Disease. *J. Hepatol.* **2018**, *69* (1), 154–181. https://doi.org/10.1016/J.JHEP.2018.03.018.

(9) Vonghia, L.; Michielsen, P.; Dom, G.; Francque, S. Diagnostic Challenges in Alcohol Use Disorder and Alcoholic Liver Disease. *World J. Gastroenterol.* **2014**, *20* (25), 8024–8032. https://doi.org/10.3748/WJG.V20.I25.8024.

(10) Su Jung, K.; Su Hee, K.; Ji Hyun, K.; Shin, H.; Hyun Ju, Y. Understanding Metabolomics in Biomedical Research. *Endocrinol. Metab.* **2016**, *31* (1), 7–16. https://doi.org/10.3803/ENM.2016.31.1.7.

(11) Brandon-Warner, E.; Schrum, L. W.; Schmidt, C. M.; McKillop, I. H. Rodent Models of Alcoholic Liver Disease: Of Mice and Men. *Alcohol* **2012**, *46* (8), 715–725. https://doi.org/10.1016/J.ALCOHOL.2012.08.004.

(12) Lamas-Paz, A.; Hao, F.; Nelson, L. J.; Vázquez, M. T.; Canals, S.; Moral, M. G. del; Martínez-Naves, E.; Nevzorova, Y. A.; Cubero, F. J. Alcoholic Liver Disease: Utility of Animal Models. *World J. Gastroenterol.* **2018**, *24* (45), 5063–5075. https://doi.org/10.3748/WJG.V24.I45.5063.

(13) Guillouzo, A.; Corlu, A.; Aninat, C.; Glaise, D.; Morel, F.; Guguen-Guillouzo, C. The Human Hepatoma HepaRG Cells: A Highly Differentiated Model for Studies of Liver Metabolism and Toxicity of Xenobiotics. *Chem. Biol. Interact.* **2007**, *168* (1), 66–73. https://doi.org/10.1016/j.cbi.2006.12.003.

(14) Marion, M.-J.; Hantz, O.; Durantel, D. The HepaRG Cell Line: Biological Properties and Relevance as a Tool for Cell Biology, Drug Metabolism, and Virology Studies. In *Methods in molecular biology*; Maurel, P., Ed.; Humana Press: United States, 2010; Vol. 640, pp 261–272. https://doi.org/10.1007/978-1-60761-688-7_13.

(15) Kell, D. B.; Brown, M.; Davey, H. M.; Dunn, W. B.; Spasic, I.; Oliver, S. G. Metabolic Footprinting and Systems Biology: The Medium Is the Message. *Nat. Rev. Microbiol.* **2005**, *3* (7), 557–565. https://doi.org/10.1038/nrmicro1177.

(16) Ates, G.; Vanhaecke, T.; Rogiers, V.; Rodrigues, R. M. Assaying Cellular Viability Using the Neutral Red Uptake Assay. In *Cell Viability Assays: Methods in Molecular Biology*; Gilbert, D. F., Friedrich, O., Eds.; Humana Press: New York, NY, 2017; pp 19–26. https://doi.org/10.1007/978-1-4939-6960-9_2.

(17) Iturrospe, E.; Da Silva, K. M.; Talavera Andújar, B.; Cuykx, M.; Boeckmans, J.; Vanhaecke, T.; Covaci, A.; van Nuijs, A. L. N. An Exploratory Approach for an Oriented Development of an Untargeted Hydrophilic Interaction Liquid Chromatography-Mass Spectrometry Platform for Polar Metabolites in Biological Matrices. *J. Chromatogr. A* **2021**, *1637*, 461807. https://doi.org/https://doi.org/10.1016/j.chroma.2020.461807.

(18) da Silva, K. M.; Iturrospe, E.; Heyrman, J.; Koelmel, J. P.; Cuykx, M.; Vanhaecke, T.; Covaci, A.; van Nuijs, A. L. N. Optimization of a Liquid Chromatography-Ion Mobility-High Resolution Mass Spectrometry Platform for Untargeted Lipidomic and Application to HepaRG Cell Extracts. *Talanta* **2021**, 122808. https://doi.org/10.1016/j.talanta.2021.122808.

(19) Maudens, K. E.; Patteet, L.; van Nuijs, A. L. N.; Van Broekhoven, C.; Covaci, A.; Neels, H. The Influence of the Body Mass Index (BMI) on the Volume of Distribution of Ethanol. *Forensic Sci. Int.* **2014**, *243*, 74–78. https://doi.org/10.1016/J.FORSCIINT.2014.04.036.

(20) Koelmel, J. P.; Kroeger, N. M.; Gill, E. L.; Ulmer, C. Z.; Bowden, J. A.; Patterson, R. E.; Yost, R. A.; Garrett, T. J. Expanding Lipidome Coverage Using LC-MS/MS Data-Dependent Acquisition with Automated Exclusion List Generation. *J. Am. Soc. Mass Spectrom.* **2017**, *28* (5), 908–917. https://doi.org/10.1007/s13361-017-1608-0.

(21) Kessner, D.; Chambers, M.; Burke, R.; Agus, D.; Mallick, P. ProteoWizard: Open Source Software for Rapid Proteomics Tools Development. *Bioinformatics* **2008**, *24* (21), 2534–2536. https://doi.org/10.1093/BIOINFORMATICS/BTN323.

(22) Tsugawa, H.; Ikeda, K.; Takahashi, M.; Satoh, A.; Mori, Y.; Uchino, H.; Okahashi, N.; Yamada, Y.; Tada, I.; Bonini, P.; Higashi, Y.; Okazaki, Y.; Zhou, Z.; Zhu, Z.-J.; Koelmel, J.; Cajka, T.; Fiehn, O.; Saito, K.; Arita, M.; Arita, M. A Lipidome Atlas in MS-DIAL 4. *Nat. Biotechnol.* **2020**, *38* (10), 1159–1163. https://doi.org/10.1038/s41587-020-0531-2.

(23) DeFelice, B. C.; Mehta, S. S.; Samra, S.; Čajka, T.; Wancewicz, B.; Fahrmann, J. F.; Fiehn, O. Mass Spectral Feature List Optimizer (MS-FLO): A Tool To Minimize False Positive Peak Reports in Untargeted Liquid Chromatography-Mass Spectroscopy (LC-MS) Data Processing. *Anal. Chem.* **2017**, *89* (6), 3250–3255. https://doi.org/10.1021/ACS.ANALCHEM.6B04372.

(24) Klåvus, A.; Kokla, M.; Noerman, S.; Koistinen, V. M.; Tuomainen, M.; Zarei, I.; Meuronen, T.; Häkkinen, M. R.; Rummukainen, S.; Babu, A. F.; Sallinen, T.; Kärkkäinen, O.; Paananen, J.; Broadhurst, D.; Brunius, C.; Hanhineva, K. "Notame": Workflow for Non-Targeted LC-MS Metabolic Profiling. *Metabolites* **2020**, *10* (4), 1–35. https://doi.org/10.3390/metabo10040135.

(25) Li, B.; Tang, J.; Yang, Q.; Cui, X.; Li, S.; Chen, S.; Cao, Q.; Xue, W.; Chen, N.; Zhu, F. Performance Evaluation and Online Realization of Data-Driven Normalization Methods Used in LC/MS Based Untargeted Metabolomics Analysis. *Sci. Rep.* **2016**, *6*, 38881. https://doi.org/10.1038/srep38881.

(26) De Livera, A. M.; Olshansky, M.; Speed, T. P. Statistical Analysis of Metabolomics Data. In *Methods in molecular biology*; Roessner, U., Dias, D., Eds.; Humana Press: Totowa, NJ, 2013; Vol. 1055, pp 291–307. https://doi.org/10.1007/978-1-62703-577-4_20.

(27) Saccenti, E.; Hoefsloot, H. C. J.; Smilde, A. K.; Westerhuis, J. A.; Hendriks, M. M. W. B. Reflections on Univariate and Multivariate Analysis of Metabolomics Data. *Metabolomics* **2014**, *10* (3), 361–374. https://doi.org/10.1007/S11306-013-0598-6.

(28) Bilbao, A.; Gibbons, B. C.; Stow, S. M.; Kyle, J. E.; Bloodsworth, K. J.; Payne, S. H.; Smith, R. D.; Ibrahim, Y. M.; Baker, E. S.; Fjeldsted, J. C. A Preprocessing Tool for Enhanced Ion Mobility-Mass Spectrometry-Based Omics Workflows. *J. Proteome Res.* **2021**. https://doi.org/10.1021/ACS.JPROTEOME.1C00425.

(29) Tsugawa, H.; Kind, T.; Nakabayashi, R.; Yukihira, D.; Tanaka, W.; Cajka, T.; Saito, K.; Fiehn, O.; Arita, M. Hydrogen Rearrangement Rules: Computational MS/MS Fragmentation and Structure Elucidation Using MS-FINDER Software. *Anal. Chem.* **2016**, *88* (16), 7946–7958. https://doi.org/10.1021/ACS.ANALCHEM.6B00770.

(30) Horai, H.; Arita, M.; Kanaya, S.; Nihei, Y.; Ikeda, T.; Suwa, K.; Ojima, Y.; Tanaka, K.; Tanaka, S.; Aoshima, K.; Oda, Y.; Kakazu, Y.; Kusano, M.; Tohge, T.; Matsuda, F.; Sawada, Y.; Hirai, M. .; Nakanishi, H.; Ikeda, K.; Akimoto, N.; Maoka, T.; Takahashi, H.; Ara, T.; Sakurai, N.; Suzuki, H.; Shibata, D.; Neumann, S.; Nishioka, T. MassBank: A Public Repository for Sharing Mass Spectral Data for Life Sciences. *J. Mass Spectrom.* **2010**, *45* (7), 703–714. https://doi.org/10.1002/JMS.1777.

(31) Smith, C. A.; O'Maille, G.; Want, E. J.; Qin, C.; Trauger, S. A.; Brandon, T. R.; Custodio, D. E.; Abagyan, R.; Siuzdak, G. METLIN: A Metabolite Mass Spectral Database. *Ther. Drug Monit.* **2005**, *27* (6), 747–751. https://doi.org/10.1097/01.ftd.0000179845.53213.39.

(32) Nothias, L.-F.; Petras, D.; Schmid, R.; Dührkop, K.; Rainer, J.; Sarvepalli, A.; Protsyuk, I.; Ernst, M.; Tsugawa, H.; Fleischauer, M.; Aicheler, F.; Aksenov, A. A.; Alka, O.; Allard, P.-M.; Barsch, A.; Cachet, X.; Caraballo-Rodriguez, A. M.; Da Silva, R. R.; Dang, T.; Garg, N.; Gauglitz, J. M.; Gurevich, A.; Isaac, G.; Jarmusch, A. K.; Kameník, Z.; Kang, K. Bin; Kessler, N.; Koester, I.; Korf, A.; Le Gouellec, A.; Ludwig, M.; Martin H., C.; McCall, L.-I.; McSayles, J.; Meyer, S. W.; Mohimani, H.; Morsy, M.; Moyne, O.; Neumann, S.; Neuweger, H.; Nguyen, N. H.; Nothias-Esposito, M.; Paolini, J.; Phelan, V. V.; Pluskal, T.; Quinn, R. A.; Rogers, S.; Shrestha, B.; Tripathi, A.; van der Hooft, J. J. J.; Vargas, F.; Weldon, K. C.; Witting, M.; Yang, H.; Zhang, Z.; Zubeil, F.; Kohlbacher, O.; Böcker, S.; Alexandrov, T.; Bandeira, N.; Wang, M.; Dorrestein, P. C. Feature-Based Molecular Networking in the GNPS Analysis Environment. *Nat. Methods* **2020**, *17* (9), 905–908. https://doi.org/10.1038/s41592-020-0933-6.

(33) Koelmel, J. P.; Kroeger, N. M.; Ulmer, C. Z.; Bowden, J. A.; Patterson, R. E.; Cochran, J. A.; Beecher, C. W. W.; Garrett, T. J.; Yost, R. A. LipidMatch: An Automated Workflow for Rule-Based Lipid Identification Using Untargeted High-Resolution Tandem Mass Spectrometry Data. *BMC Bioinformatics* **2017**, *18* (1), 331.

https://doi.org/10.1186/s12859-017-1744-3.

(34) Ni, Z.; Angelidou, G.; Lange, M.; Hoffmann, R.; Fedorova, M. LipidHunter Identifies Phospholipids by High-Throughput Processing of LC-MS and Shotgun Lipidomics Datasets. *Anal. Chem.* **2017**, *89* (17), 8800–8807. https://doi.org/10.1021/ACS.ANALCHEM.7B01126.

(35) Pi, J.; Wu, X.; Feng, Y. Fragmentation Patterns of Five Types of Phospholipids by Ultra-High-Performance Liquid Chromatography Electrospray Ionization Quadrupole Time-of-Flight Tandem Mass Spectrometry. *Anal. Methods* **2016**, *8* (6), 1319–1332. https://doi.org/10.1039/C5AY00776C.

(36) Lange, M.; Angelidou, G.; Ni, Z.; Criscuolo, A.; Schiller, J.; Blüher, M.; Fedorova, M. AdipoAtlas: A Reference Lipidome for Human White Adipose Tissue. *Cell Reports Med.* **2021**, *2* (10), 100407. https://doi.org/10.1016/J.XCRM.2021.100407.

(37) Schymanski, E. L.; Jeon, J.; Gulde, R.; Fenner, K.; Ruff, M.; Singer, H. P.; Hollender, J. Identifying Small Molecules via High Resolution Mass Spectrometry: Communicating Confidence. *Environ. Sci. Technol.* **2014**, *48* (4), 2097–2098. https://doi.org/10.1021/es5002105.

(38) Zhou, Z.; Luo, M.; Chen, X.; Yin, Y.; Xiong, X.; Wang, R.; Zhu, Z. J. Ion Mobility Collision Cross-Section Atlas for Known and Unknown Metabolite Annotation in Untargeted Metabolomics. *Nat. Commun.* **2020**, *11* (1), 1–13. https://doi.org/10.1038/s41467-020-18171-8.

(39) Naz, S.; Vallejo, M.; García, A.; Barbas, C. Method Validation Strategies Involved in Non-Targeted Metabolomics. *J. Chromatogr. A* **2014**, *1353*, 99–105. https://doi.org/10.1016/j.chroma.2014.04.071.

(40) Wang, F.; Liigand, J.; Tian, S.; Arndt, D.; Greiner, R.; Wishart, D. S. CFM-ID 4.0: More Accurate ESI-MS/MS Spectral Prediction and Compound Identification. *Anal. Chem.* **2021**, *93* (34), 11692–11700. https://doi.org/10.1021/ACS.ANALCHEM.1C01465.

(41) Lieber, C. S.; Robins, S. J.; Leo, M. A. Hepatic Phosphatidylethanolamine Methyltransferase Activity Is Decreased by Ethanol and Increased by Phosphatidylcholine. *Alcohol. Clin. Exp. Res.* **1994**, *18* (3), 592–595. https://doi.org/10.1111/J.1530-0277.1994.TB00915.X.

(42) Jaremek, M.; Yu, Z.; Mangino, M.; Mittelstrass, K.; Prehn, C.; Singmann, P.; Xu, T.; Dahmen, N.; Weinberger, K. M.; Suhre, K.; Peters, A.; Döring, A.; Hauner, H.; Adamski, J.; Illig, T.; Spector, T. D.; Wang-Sattler, R. Alcohol-Induced Metabolomic Differences in Humans. *Transl. Psychiatry* **2013**, *3* (7), e276–e276. https://doi.org/10.1038/tp.2013.55.

(43) Aroor, A. R.; Custer, G. W.; Weng, Y. I.; Lee, Y. J.; Shukla, S. D. Phosphatidylethanol Mimics Ethanol Modulation of P42/44 Mitogen-Activated Protein Kinase Signalling in Hepatocytes. *Alcohol Alcohol.* **2002**, *37* (6), 534–539. https://doi.org/10.1093/ALCALC/37.6.534.

(44) Stickel, F.; Seitz, H. Ethanol and Methyl Transfer. In *Nutrition and Alcohol*; Watson, R. R., Preedy, V. R., Eds.; CRC Press: New York, NY, 2003; pp 57–71. https://doi.org/10.1201/9780203507636.CH4.

(45) Ganesan, M.; Feng, D.; Barton, R. W.; Thomes, P. G.; McVicker, B. L.; Tuma, D. J.; Osna, N. A.; Kharbanda, K. K. Creatine Supplementation Does Not Prevent the Development of Alcoholic Steatosis. *Alcohol. Clin. Exp. Res.* **2016**, *40* (11), 2312–2319. https://doi.org/10.1111/ACER.13214.

(46) Wang, Z.; Yao, T.; Song, Z. Involvement and Mechanism of DGAT2 Upregulation in the Pathogenesis of

Alcoholic Fatty Liver Disease. *J. Lipid Res.* **2010**, *51* (11), 3158–3165. https://doi.org/10.1194/JLR.M007948.

(47) Hu, M.; Wang, F.; Li, X.; Rogers, C. Q.; Liang, X.; Finck, B. N.; Mitra, M. S.; Zhang, R.; Mitchell, D. A.; You, M. Regulation of Hepatic Lipin-1 by Ethanol: Role of AMP-Activated Protein Kinase/Sterol Regulatory Element-Binding Protein 1 Signaling in Mice. *Hepatology* **2012**, *55* (2), 437–446. https://doi.org/10.1002/HEP.24708.

(48) Hu, M.; Yin, H.; Mitra, M. S.; Liang, X.; Ajmo, J. M.; Nadra, K.; Chrast, R.; Finck, B. N.; You, M. Hepatic-Specific Lipin-1 Deficiency Exacerbates Experimental Alcohol-Induced Steatohepatitis in Mice. *Hepatology* **2013**, *58* (6), 1953–1963. https://doi.org/10.1002/HEP.26589.

(49) Jeon, S.; Carr, R. Alcohol Effects on Hepatic Lipid Metabolism. *J. Lipid Res.* **2020**, *61* (4), 470–479. https://doi.org/10.1194/JLR.R119000547.

(50) Israelsen, M.; Kim, M.; Suvitaival, T.; Madsen, B. S.; Hansen, C. D.; Torp, N.; Trost, K.; Thiele, M.; Hansen, T.; Legido-Quigley, C.; Krag, A. Comprehensive Lipidomics Reveals Phenotypic Differences in Hepatic Lipid Turnover in ALD and NAFLD during Alcohol Intoxication. *JHEP Reports* **2021**, *3* (5), 100325. https://doi.org/10.1016/J.JHEPR.2021.100325.

(51) Puri, P.; Xu, J.; Vihervaara, T.; Katainen, R.; Ekroos, K.; Daita, K.; Min, H. K.; Joyce, A.; Mirshahi, F.; Tsukamoto, H.; Sanyal, A. J. Alcohol Produces Distinct Hepatic Lipidome and Eicosanoid Signature in Lean and Obese. *J. Lipid Res.* **2016**, *57* (6), 1017–1028. https://doi.org/10.1194/JLR.M066175.

(52) Koelmel, J. P.; Tan, W. Y.; Li, Y.; Bowden, J. A.; Ahmadireskety, A.; Patt, A. C.; Orlicky, D. J.; Mathé, E.; Kroeger, N. M.; Thompson, D. C.; Cochran, J. A.; Golla, J. P.; Kandyliari, A.; Chen, Y.; Charkoftaki, G.; Guingab-Cagmat, J. D.; Tsugawa, H.; Arora, A.; Veselkov, K.; Kato, S.; Otoki, Y.; Nakagawa, K.; Yost, R. A.; Garrett, T. J.; Vasilou, V. Lipidomics and Redox Lipidomics Indicate Early Stage Alcohol-Induced Liver Damage. *Hepatol. Commun.* **2021**. https://doi.org/10.1002/HEP4.1825.

(53) Puri, P.; Baillie, R. A.; Wiest, M. M.; Mirshahi, F.; Choudhury, J.; Cheung, O.; Sargeant, C.; Contos, M. J.; Sanyal, A. J. A Lipidomic Analysis of Nonalcoholic Fatty Liver Disease. *Hepatology* **2007**, *46* (4), 1081–1090. https://doi.org/10.1002/HEP.21763.

(54) Myoung, S. H.; Sun, Y. P.; Shinzawa, K.; Kim, S.; Kun, W. C.; Lee, J. H.; Choon, H. K.; Lee, K. W.; Lee, J. H.; Cheol, K. P.; Woo, J. C.; Jae, S. H.; Yan, J. J.; Song, D. K.; Tsujimoto, Y.; Lee, M. S. Lysophosphatidylcholine as a Death Effector in the Lipoapoptosis of Hepatocytes. *J. Lipid Res.* **2008**, *49* (1), 84–97. https://doi.org/10.1194/JLR.M700184-JLR200.

(55) Stefanescu, H.; Suciu, A.; Romanciuc, F.; Crisan, D.; Procopet, B.; Radu, C.; Tantau, M.; Socaciu, C.; Grigorescu, M. Lyso-Phosphatidylcholine: A Potential Metabolomic Biomarker for Alcoholic Liver Disease? *Hepatology* **2016**, *64* (2), 678–679. https://doi.org/10.1002/HEP.28630/SUPPINFO.

(56) Li, Z.; Agellon, L. B.; Vance, D. E. Phosphatidylcholine Homeostasis and Liver Failure. *J. Biol. Chem.* **2005**, *280* (45), 37798–37802. https://doi.org/10.1074/JBC.M508575200.

(57) Cuykx, M.; Claes, L.; Rodrigues, R. M.; Vanhaecke, T.; Covaci, A. Metabolomics Profiling of Steatosis Progression in HepaRG® Cells Using Sodium Valproate. *Toxicol. Lett.* **2018**, *286*, 22–30. https://doi.org/10.1016/j.toxlet.2017.12.015.

(58) Calzada, E.; Onguka, O.; Claypool, S. M. Phosphatidylethanolamine Metabolism in Health and Disease. *Int. Rev. Cell Mol. Biol.* **2016**, *321*, 29–88. https://doi.org/10.1016/BS.IRCMB.2015.10.001.

(59) Pavlovic, Z.; Bakovic, M. Regulation of Phosphatidylethanolamine Homeostasis—The Critical Role of CTP:Phosphoethanolamine Cytidylyltransferase (Pcyt2). *Int. J. Mol. Sci.* **2013**, *14* (2), 2529–2550. https://doi.org/10.3390/IJMS14022529.

(60) Ma, X.; Qian, H.; Chen, A.; Ni, H. M.; Ding, W. X. Perspectives on Mitochondria–ER and Mitochondria–Lipid Droplet Contact in Hepatocytes and Hepatic Lipid Metabolism. *Cells* **2021**, *10* (9), 2273. https://doi.org/10.3390/CELLS10092273.

(61) van der Veen, J. N.; Kennelly, J. P.; Wan, S.; Vance, J. E.; Vance, D. E.; Jacobs, R. L. The Critical Role of Phosphatidylcholine and Phosphatidylethanolamine Metabolism in Health and Disease. *Biochim. Biophys. Acta - Biomembr.* **2017**, *1859* (9), 1558–1572. https://doi.org/10.1016/J.BBAMEM.2017.04.006.

(62) Skaff, O.; Pattison, D. I.; Davies, M. J. The Vinyl Ether Linkages of Plasmalogens Are Favored Targets for Myeloperoxidase-Derived Oxidants: A Kinetic Study†. *Biochemistry* **2008**, *47* (31), 8237–8245. https://doi.org/10.1021/BI800786Q.

(63) Dean, J. M.; Lodhi, I. J. Structural and Functional Roles of Ether Lipids. *Protein Cell* **2018**, *9* (2), 196–206. https://doi.org/10.1007/S13238-017-0423-5.

(64) Wu, G.; Yang, J.; Lv, H.; Jing, W.; Zhou, J.; Feng, Y.; Lin, S.; Yang, Q.; Hu, J. Taurine Prevents Ethanol-Induced Apoptosis Mediated by Mitochondrial or Death Receptor Pathways in Liver Cells. *Amino Acids* **2018**, *50* (7), 863–875. https://doi.org/10.1007/S00726-018-2561-3/FIGURES/7.

(65) Liu, J. J.; Wang, J. Y.; Hertervig, E.; Cheng, Y.; Nilsson, Å. K. E.; Duan, R. D. Activation of Neutral Sphingomyelinase Participates in Ethanol-Induced Apoptosis in Hep G2 Cells. *Alcohol Alcohol* **2000**, *35* (6), 569–573. https://doi.org/10.1093/ALCALC/35.6.569.

(66) Yang, L.; Jin, G. H.; Zhou, J. Y. The Role of Ceramide in the Pathogenesis of Alcoholic Liver Disease. *Alcohol Alcohol.* **2016**, *51* (3), 251–257. https://doi.org/10.1093/ALCALC/AGV119.

(67) Liangpunsakul, S.; Sozio, M. S.; Shin, E.; Zhao, Z.; Xu, Y.; Ross, R. A.; Zeng, Y.; Crabb, D. W. Inhibitory Effect of Ethanol on AMPK Phosphorylation Is Mediated in Part through Elevated Ceramide Levels. *Am. J. Physiol. - Gastrointest. Liver Physiol.* **2010**, *298* (6), 1004–1012. https://doi.org/10.1152/AJPGI.00482.2009/ASSET/IMAGES/LARGE/ZH30061056460006.JPEG.

(68) Savic, D.; Hodson, L.; Neubauer, S.; Pavlides, M. The Importance of the Fatty Acid Transporter L-Carnitine in Non-Alcoholic Fatty Liver Disease (NAFLD). *Nutrients* **2020**, *12* (8), 1–17. https://doi.org/10.3390/NU12082178.

(69) Li, N.; Zhao, H. Role of Carnitine in Non-Alcoholic Fatty Liver Disease and Other Related Diseases: An Update. *Front. Med.* **2021**, *8*, 689042. https://doi.org/10.3389/FMED.2021.689042.

(70) Gao, B.; Bataller, R. Alcoholic Liver Disease: Pathogenesis and New Therapeutic Targets. *Gastroenterology* **2011**, *141* (5), 1572–1585. https://doi.org/10.1053/J.GASTRO.2011.09.002.

(71) Machado, M. V.; Kruger, L.; Jewell, M. L.; Michelotti, G. A.; Pereira, T. de A.; Xie, G.; Moylan, C. A.; Diehl, A. M. Vitamin B5 and N-Acetylcysteine in Nonalcoholic Steatohepatitis: A Pre-Clinical Study in a Dietary

Mouse Model. *Dig. Dis. Sci.* **2016**, *61* (1), 137–148. https://doi.org/10.1007/S10620-015-3871-X.

(72) Miyazaki, A.; Sano, M.; Fukuwatari, T.; Shibata, K. Effects of Ethanol Consumption on the B-Group Vitamin Contents of Liver, Blood and Urine in Rats. *Br. J. Nutr.* **2012**, *108* (6), 1034–1041. https://doi.org/10.1017/S0007114511006192.

(73) Iannucci, J.; Milner, R.; Arbizo, M. V.; Smith, C. M. The Effect of Ethanol and Acetaldehyde on [14C]Pantothenate Incorporation into CoA in Cultured Rat Liver Parenchymal Cells. *Arch. Biochem. Biophys.* **1982**, *217* (1), 15–29. https://doi.org/10.1016/0003-9861(82)90474-X.

(74) Onofrj, M.; Ciccocioppo, F.; Varanese, S.; Di Muzio, A.; Calvani, M.; Chiechio, S.; Osio, M.; Thomas, A. Acetyl-L-Carnitine: From a Biological Curiosity to a Drug for the Peripheral Nervous System and Beyond. *Expert Rev. Neurother.* **2014**, *13* (8), 925–936. https://doi.org/10.1586/14737175.2013.814930.

(75) Steiber, A.; Kerner, J.; Hoppel, C. L. Carnitine: A Nutritional, Biosynthetic, and Functional Perspective. *Mol. Aspects Med.* **2004**, *25* (5–6), 455–473. https://doi.org/10.1016/J.MAM.2004.06.006.

(76) Nikolaou, N.; Gathercole, L. L.; Marchand, L.; Althari, S.; Dempster, N. J.; Green, C. J.; van de Bunt, M.; McNeil, C.; Arvaniti, A.; Hughes, B. A.; Sgromo, B.; Gillies, R. S.; Marschall, H. U.; Penning, T. M.; Ryan, J.; Arlt, W.; Hodson, L.; Tomlinson, J. W. AKR1D1 Is a Novel Regulator of Metabolic Phenotype in Human Hepatocytes and Is Dysregulated in Non-Alcoholic Fatty Liver Disease. *Metabolism* **2019**, *99*, 67–80. https://doi.org/10.1016/J.METABOL.2019.153947.

(77) Tascher, G.; Burban, A.; Camus, S.; Plumel, M.; Chanon, S.; Guevel, R. Le; Shevchenko, V.; Dorsselaer, A. Van; Lefai, E.; Guguen-Guillouzo, C.; Bertile, F. In-Depth Proteome Analysis Highlights HepaRG Cells as a Versatile Cell System Surrogate for Primary Human Hepatocytes. *Cells* **2019**, *8* (2), 192. https://doi.org/10.3390/CELLS8020192.